



**Acoustics'08
Paris**
June 29-July 4, 2008

www.acoustics08-paris.org

Fluctuations under turbulent flows: enhanced methods for separation of propagative wavenumbers from wall pressure dataset

Sébastien Debert^a, Marc Pachebat^a, Vincent Valeau^b and Yves Gervais^b

^aPSA-Peugeot-Citroën, Route de Gizy, CC : VV013 - Bât. 14, F-78943 Vélizy-Villacoublay
Cedex, France

^bLaboratoire d'Etudes Aérodynamiques (LEA), Université de Poitiers - ENSMA - CNRS,
Bâtiment K, 40 Avenue du Recteur Pineau, F-86022 Poitiers, France
sebastien.debert@mpsa.com

This work is a part of a more general study on automobile interior noise due to acoustic and aerodynamic wall-pressure fluctuations. Using experimental data of wall-pressure fluctuations measured with a microphone array beneath several kinds of flows, a wave-number analysis based on recently developed signal processing methods – the spatial Empirical Mode Decomposition (sEMD) and the Ensemble Empirical Mode Decomposition (E-EMD) – is carried out, in order to separate acoustic and aerodynamic pressure fluctuations. This is a first step in order to propose new methods that do not require any hypothesis (*e.g.* stationarity, uniformity) on the wall-pressure field, in opposition with classical method like the spatial correlogram. A turbulent boundary layer on a flat plate and a detached/reattached flow downstream three different forward-facing steps are tested, with flow velocities from 0 to 40 m.s⁻¹, with or without a well-controlled artificial acoustic source.

The sEMD method is first used as a wavenumber filter, and is shown to improve the detection of acoustic fluctuations of about 5 dB on classical wavenumber (k, f) representations. This studies allows us to identify the E-EMD as a good method to decompose the (x, t) representation to make possible the separation of the acoustic and aerodynamic components, regardless of the stationarity or the uniformity of the flow.

1 Introduction

The present study deals with the automobile interior noise induced by acoustic and aerodynamic wall-pressure fluctuations. It aims at separating from the turbulent energy the acoustic energy produced by turbulent flows near a wall. This separation is known to be crucial for predicting interior noise in transportation vehicle since the motion of solid structures acts as a wavenumber filter for the wall-pressure fluctuations. In the study, wall-pressure fluctuations are measured on a flat plate, behind a forward-facing step and on a side window of a real vehicle in streamwise and spanwise directions, in an anechoic Eiffel-type wind tunnel.

Firstly, a spatial correlogram approach for a 40 m.s⁻¹ flow velocity Turbulent Boundary Layer (noted further “TBL”) with a thickness of about 18 mm is shown to be incapable to separate acoustic from turbulent energy in the wavenumber-frequency plane: the acoustic energy produced by the TBL is not detectable within the noise and the artifacts of the computed wavenumber representation [2]. To our knowledge, only Arguillat *et al.* [1] had been able to make this separation using a similar spatial correlogram method, but on a 44 m.s⁻¹ flow velocity and a 120 mm-thick TBL.

The second stage consists in increasing the separation capabilities of the spatial correlogram by taking advantage of the Empirical Mode Decomposition (EMD) properties [6]. The EMD is used in an original manner along the spatial extension of the antenna to obtain new wall-pressure time signals for which the turbulence-induced small spatial oscillations are filtered out at each instant. The spatial filtering with EMD (sEMD) is described. Its capabilities are first tested for the TBL combined with acoustic energy injected by an artificial source into the wind tunnel, then applied on wall-pressure fluctuations of flows without artificial source.

2 Experimental measurements of pressure fluctuations

2.1 The TBL flow configuration

Experiments were carried out in an open anechoic wind-tunnel. The test section is located in an anechoic room, upstream to the fan. Small inserts (open diameter of

0.8 mm, spacing 5.26 mm, span 310 mm) are located in a flat plate under the turbulent flow, forming two linear arrays in the streamwise and spanwise directions, with 64 sensors each. Only results of the streamwise-line are presented here. The fully developed TBL parameters are [7]: thickness $\delta = 18$ mm, displacement thickness $\delta_1 = 2.6$ mm, momentum thickness $\theta = 2.0$ mm, energy thickness $\delta_3 = 3.7$ mm, and the first shape factor $H = \delta_1/\theta$ is 1.3. Three flow speeds (noted U_∞) are used ($U_\infty = 20, 30$ or 40 m.s⁻¹). Only results for 40 m.s⁻¹-flows are presented.

Because of the low energetic level of the acoustic contribution of the TBL flow, an artificial acoustic source is used to test the techniques for separating the acoustic and aerodynamic pressure components. This monopolar acoustic source is located upstream to the linear array.

2.2 The detached/reattached flow configurations

Two studies of detached/reattached flows are carried out. A forward-facing step (noted “M3D” further) producing a three-dimensional flow is used in the open wind-tunnel, with the same flow speeds than the TBL (see Fig. 1). The M3D step is symmetric with regard to the median axis, presenting a “double” yaw-angle of $\pm 10^\circ$ and a inclination-angle of 30° with regard to the normal of the $z = 0$ -plan. The step is 40 mm thick (about 2.5δ). This kind of step is known to provides a non-symmetric, non-stationary and non-uniform flow. The same probes than those previously described are used, forming a 61-sensors-streamwise-linear array. The same monopolar acoustic source than for the TBL case is used, but is now located beside the flow and the linear array.

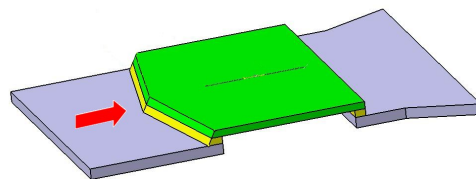


Figure 1: Configuration of the “M3D” step. The 40 m.s⁻¹ detached/reattached flow follows the red arrow.

The second study is carried out on the side window of a real vehicle in an anechoic wind-tunnel under a 38.9 m.s^{-1} flow (140 km.h^{-1}). A 64-sensors-streamwise-linear array is located behind the position of the rear-view mirror on the side-window.

3 Wavenumber representation

3.1 The spatial correlogram method

In order to estimate the streamwise wavenumber frequency spectrum $\Phi(k_x, f)$ of the wall-pressure fluctuations, a spatial correlogram method is used [4]:

$$\Phi(k_x, f) = \int_{-\infty}^{\infty} S_{ij}(x, f) e^{-jk_x \cdot x} dx, \quad (1)$$

with:

$$S_{ij}(x, f) = \text{E} \left[\int_{-\infty}^{\infty} p_i(x_i, t) p_j^*(x_i + x, t + \tau) e^{-j2\pi f \tau} d\tau \right], \quad (2)$$

where $\text{E}[\cdot]$ is the expected value and the $*$ symbol denotes the complex conjugate operator. First, the cross-power spectra (XSP) $S_{ij}(x, f)$ are computed (Eq (2)) using 300 blocks for the averaging process. The wavenumber - frequency spectra $\Phi(k_x, f)$ are then obtained by a spatial Fourier transform on the XSP (Eq (1)).

Due to the averaging process across time blocks, the correlogram method requires the hypothesis of ergodicity. In theory, the method can then be applied only to a stationary and uniform flow, as the TBL.

The modulus $|\Phi(k_x, f)|$ of the wavenumber frequency spectra for the TBL, the M3D and the vehicle are shown respectively in Fig. 2.a, 3.a and 4 in dB scale (*ref.* 1 Pa^2). Whatever its direction of propagation, all acoustic energy present in the wind-tunnel should be physically located inside a vertical cone delimited by $\pm c_0/2\pi$ slopes ($c_0 = 340 \text{ m.s}^{-1}$ is the sound velocity). The upstream artificial acoustic contribution is indeed visible in Fig. 2.a and 3.a in this zone along a straight line of slope $+c_0/2\pi$. The convective energy is mainly located as expected around a straight line with a $U_w/2\pi$ slope (U_w being the flow speed near the wall, about $0.8U_\infty$ [7]).

In Fig. 2.a, we can point out:

- the truncation effects due to the finite length of the antenna, visible for $f < 1500 \text{ Hz}$ and characterized by the energy spreading along the k_x axis at $f = 0$;
- the aliasing of convective energy specially at high frequencies ($f > 2000 \text{ Hz}$) for $k_x < 0$.

It can be noticed that artificial acoustic energy cannot be visually located below 1200 Hz as it is buried into noise and convective energy. No acoustic energy produced by the TBL itself can be seen in Fig. 2.a. Indeed, the acoustic energy signature of a diffuse sound field (which would be a vertical cone as described above) does not appear in the vicinity of the vertical axis. Only the signature of the artificial source appears. In opposition to the results of Arguillat *et al.* [1] obtained in a blowing wind tunnel with a guided flow and a TBL thickness $\delta = 120 \text{ mm}$, the acoustic energy produced by the TBL is not detected here, with a Eiffel-type open wind tunnel with downstream fan and a thinner TBL. This point should be studied further.

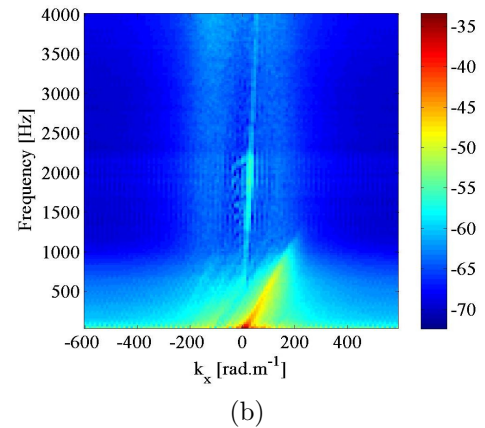
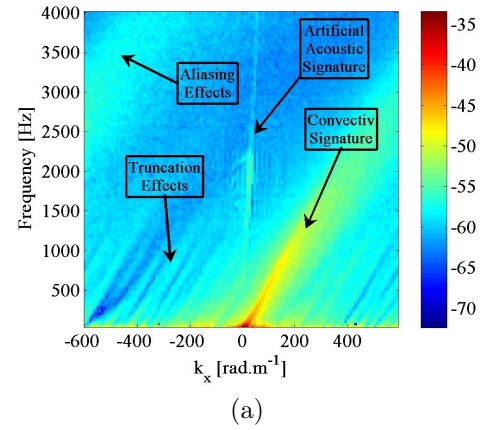


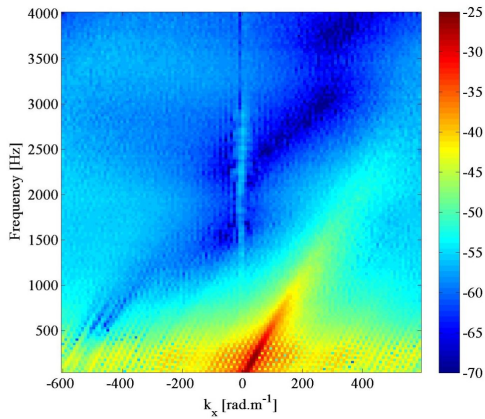
Figure 2: Modulus (dB scale) of the wavenumber spectrum in the streamwise direction beneath the TBL ($U_\infty = 40 \text{ m.s}^{-1}$), with added artificial broadband acoustic source upstream in the wind tunnel: (a) original signals, (b) sEMD-filtered signals.

Although the assumptions of uniformity and stationarity are not respected in the facing step and full-scale vehicle configurations, the spatial correlogram method is applied to the M3D and side-window configurations. In Fig. 3.a, the global energetic level is higher than the level of the TBL, which is in agreement with the higher rate of turbulence of the M3D case. Particularly, low frequencies are enhanced. The signature of the artificial acoustic source is visible only in the mid-frequency range $[1000; 3000] \text{ Hz}$, due to the effects mentioned above (truncation and aliasing of convective energy).

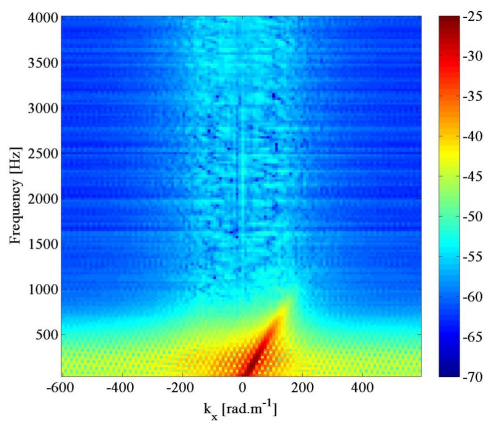
Finally in Fig. 4, the same observations can be made on the vehicle-side-window case concerning the high energetic level at low frequency, the truncation effects and the aliasing effects. Furthermore, as no artificial acoustic source is used here, no acoustical signature is detectable in the theoretical acoustic cone.

3.2 Conclusion on the spatial correlogram method

The application of the spatial correlogram method to pressure fluctuation signals under a Turbulent Boundary Layer in an anechoic open wind tunnel shows that acoustic fluctuations induced by turbulence cannot be separated from turbulent energy in our case of a TBL-thickness of 18 mm , a result which is in opposition with



(a)



(b)

Figure 3: Modulus (dB scale) of the wavenumber spectrum in the streamwise direction beneath the detached/reattached flow downstream the forward-facing steps (M3D configuration, $U_\infty = 40 \text{ m.s}^{-1}$), with added artificial broadband acoustic source beside the flow in the wind tunnel: (a) original signals, (b) sEMD-filtered signals.

Arguillat *et al.* [1]. Furthermore, on non-uniform non-stationary flows, the acoustical signature of the flow remains not detectable. A new method based on Empirical Mode Decomposition in the spatial domain is now presented and used as a low-pass filtering technique to improve the separation of convective and propagative wavenumbers.

4 Low-pass filtering in the spatial domain at each instant

4.1 The Empirical Mode Decomposition (EMD)

As an example to present the EMD, a signal $x(t)$ will be now used, which can be a temporal or spatial signal. The EMD considers a signal at the scale of its local oscillations by formally writing that locally: “signal = fast oscillations superimposed to slow oscillations”. Looking at a single local oscillation (defined, e.g. as the signal between two consecutive local minima), the EMD is designed to define a local “low frequency” component

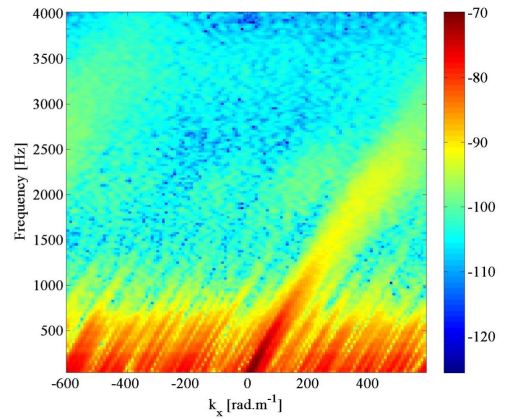


Figure 4: Modulus (dB scale) of the wavenumber spectrum in the streamwise direction beneath the detached/reattached flow on the side window of a vehicle ($U_\infty = 140 \text{ km.h}^{-1}$) in a full scale anechoic wind tunnel.

as the *local trend* $m_1(t)$, supporting a local “high frequency” component as a zero-mean oscillation or *local detail* $d_1(t)$, with: $x(t) = m_1(t) + d_1(t)$. By construction, $d_1(t)$ is an oscillatory signal and $m_1(t)$ oscillates slower than $d_1(t)$. If we build $d_1(t)$ to be locally zero-mean everywhere, it corresponds to what is referred to as an *Intrinsic Mode Function* (IMF) [6]. This implies that all its maxima (resp. minima) are positive (resp. negative). Applying recursively this decomposition to $m_i(t)$ is called the *sifting process*, and gives an *Empirical Mode Decomposition* of the original signal as follows:

$$x(t) = m_K(t) + \sum_{k=1}^K d_k(t), \quad (3)$$

where $m_K(t)$ is the final *residue* of the decomposition. Before using the *Empirical Mode Decomposition*, we must point out that it is not unique as the IMFs depend on parameters used in the sifting algorithm, but yields to IMFs that are nearly perfectly orthogonal. At a given instant, one particular frequency component of the original signal $x(t)$ is represented by one and only one IMF in the decomposition. Removing out some of the first IMFs (say e.g. $d_1(t)$ and $d_2(t)$) from Eq (3) can be similar to low-pass filtering $x(t)$ [3].

4.2 The Empirical Mode Decomposition to enhance the spatial correlogram

In order to enhance the detection of acoustic energy existing at low wavenumbers (near the vertical axis $k_x = 0$), one have to decrease turbulent energy and improve the signal-to-noise ratio by avoiding the truncation and aliasing effects (Fig. 2). The low-pass filtering is performed by the EMD¹ in the spatial domain (called here “sEMD”) of the $N = 2.56 \cdot 10^6$ instant realizations of the wall-pressure spatial signal along the linear array [5]. An example of the decomposition of one instantaneous spatial signal is shown in Fig. 5: as expected by the

¹computer codes used here for the Empirical Mode Decomposition are available at the following address: <http://perso.ens-lyon.fr/patrick.flandrin/emd.html>.

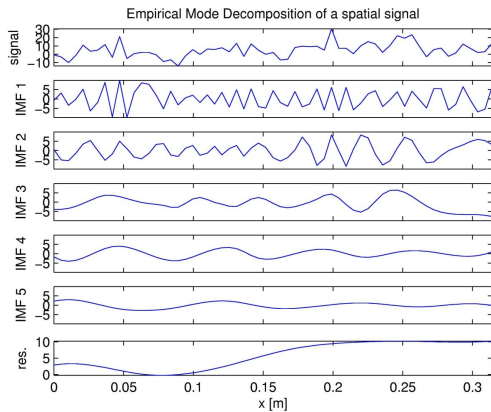


Figure 5: Decomposition into spatial IMF of the instantaneous wall-pressure fluctuations measured along the streamwise array (TBL, $U_\infty = 40 \text{ m.s}^{-1}$). From top to bottom: original signal, IMF₁ (highest wavenumbers) to IMF₅ (low wavenumbers), and residue (trend).

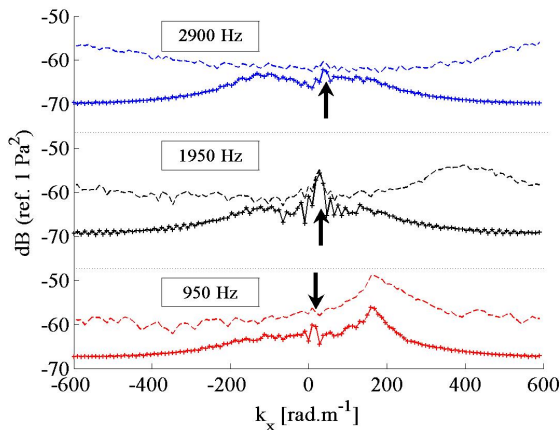


Figure 6: Comparison of Fig. 2.a and Fig. 2.b at three frequencies (dB ref. 1 Pa^2) for the TBL configuration. Dashed line: original signals, solid line: sEMD-filtered signals. The arrow indicates the theoretical position of the acoustic peak.

algorithm, higher (spatial-)frequencies (*i.e.*, high wavenumbers) can be found in the first modes. The residue is just a trend with no oscillation, only one extremum (which is here a minimum).

Below 4000 Hz, the acoustic wavenumbers $k_x = \omega/c_0$ are included in the range $[-74; 74] \text{ rad.m}^{-1}$. Assuming that the zero-crossing number of an IMF is a rough estimation of its mean spatial frequency, we can associate this number to a wavenumber. The minimum zero-crossing number of the two first IMFs is always superior to 13, and thus corresponds to a wavenumber about 120 rad.m^{-1} which is much higher than the maximum acoustic wavenumber. This ensures that removing the two first IMFs keeps the acoustic energy intact for $f < 4000 \text{ Hz}$. The removing of the two first IMFs is then repeated N times (for each of the N instant realisations of the spatial signal).

Results of sEMD processing on wall-pressure fluctuations are shown in Fig. 2.b. Comparison between Fig. 2.a and Fig. 2.b confirms, as expected, that removing the two first IMFs acts as a low-pass filtering in the wave-

number domain. Indeed, the energy located in the wavenumber domain beyond $\pm 150 \text{ rad.m}^{-1}$ is considerably attenuated. But low-pass sEMD-filtering also leads to the enhancement of the acoustic signal-to-noise ratio in the vicinity of the vertical axis (near $k_x = 0$). In particular, the “acoustic line” due to the artificial noise source is now visible in the $[700; 1200] \text{ Hz}$ frequency range in Fig. 2.b. This shows that sEMD is more efficient than a simple low-pass wavenumber filtering.

To confirm this analysis, Fig. 6 plots, at different frequencies, the sections of the modulus of the wavenumber-frequency spectra of Fig. 2 (TBL case), before and after sEMD. On original signals (dashed lines), the turbulent signature is easily noticed at about $k = 200, 400$ and $+600/-600 \text{ rad.m}^{-1}$ respectively for $f = 950, 1950$ and 2900 Hz . The theoretical position of the acoustic signature is indicated with the arrow. The acoustic peak is hardly detectable for $f = 950 \text{ Hz}$ and $f = 2900 \text{ Hz}$, and is well visible for $f = 1950 \text{ Hz}$. It appears that after sEMD, the convective energy is well reduced beyond $\pm 150 \text{ rad.m}^{-1}$ and the convective energy due to truncation and aliasing effects is also canceled all over the wavenumber range (this is particularly visible for $f = 950 \text{ Hz}$). The (artificial) acoustic energy can then be extracted from noise (for $f = 950 \text{ Hz}$ and $f = 2900 \text{ Hz}$). Furthermore, the $f = 1950 \text{ Hz}$ -sections allow us to assert that this acoustic energy remains intact after the sEMD filtering, as both before and after peaks are identical.

Although it allows us to increase the separation capabilities of the spatial correlogram, this sEMD method is not sufficient to extract the Turbulent Boundary Layer noise itself. It is now used on a non-stationary and non-uniform flow behind a forward-facing step, for which the acoustic energetic level is expected to be higher.

5 Application of the spatial EMD (sEMD) to a non-uniform non-stationary flow

Results of sEMD processing on “M3D” wall-pressure fluctuations are shown in Fig. 3.b. As for the TBL configuration, the low-pass filtering in the wave domain is effective. The cutoff wavenumber is about $\pm 150 \text{ rad.m}^{-1}$, ensuring that all the acoustic energy is preserved in this frequency range. Beyond this wavenumber, the effects of truncation and aliasing are totally cancelled. But for small wavenumbers, no enhancement of the acoustic signal-to-noise ratio is observed: the “acoustic line” can hardly be detected. Using a similar analysis than for Fig. 6, the sections before and after sEMD in Fig. 7 confirm that beyond the cutoff wavenumber, the energy is decreased. On the other hand, in the vicinity of the vertical axis, sEMD seems to increase the global energy. At low frequency ($f = 950 \text{ Hz}$), no increase but no improvement neither is observed. For higher frequencies, an increase about 5 dB is noticed. The peak of the artificial acoustic contribution can still be observed, but does not appear clearly from the ambient level. The sEMD technique seems to be inappropriate for analysing this kind of non-uniform and non-stationary flow.

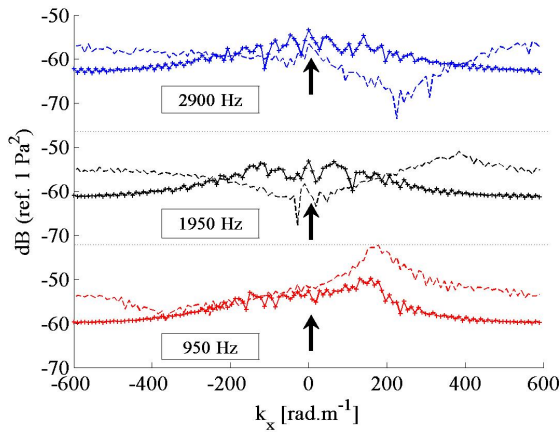


Figure 7: Comparison of Fig. 3.a and Fig. 3.b at three frequencies (dB *ref.* 1 Pa²) for the M3D configuration. Dashed line: original signals, solid line: sEMD-filtered signals. The arrow indicates the theoretical position of the acoustic peak.

However, the representations used here are still the result of the spatial correlogram method, which require the ergodic hypothesis that a non-uniform and non-stationary flow does not respect. Thus, the increase of the energy around the cutoff-wavenumbers could be a consequence of the combination of filtering and averaging. Another kind of representation (instantaneous representation) is needed that does not require the ergodic hypothesis.

The Ensemble-EMD (E-EMD) technique [8] could allow us to follow each IMF of the decomposition across the time dimension. Indeed, sEMD provides a variable number of IMFs for each instant decomposition, preventing from following each mode across time. The E-EMD allows to obtain a constant number of IMFs. This consists in adding white noise to the (spatial) signal, in applying the EMD technique, in keeping only the decompositions that have a chosen number of IMFs, and then in repeating this process to obtain a sufficient number of decompositions (typically about a thousand decompositions), in order to cancel the contribution of the white noise by averaging each IMF. This whole process is repeated for each realisation N . With a constant number of IMFs for each instant, each IMF is constituted by the same range of wavenumbers across time. It is then possible to perform operations (like Fourier Transform to obtain energetic spectrum) on chosen range of wavenumbers. Knowing this range of wavenumbers gives the theoretical frequency where the acoustic peak lies. Thus, for each IMFs, a energy spectrum could allow us to estimate a dynamic energetic threshold below which the acoustic contribution energy lies at each instant.

6 Conclusion

Applying the spatial correlogram to pressure fluctuations in an anechoic open wind tunnel shows that in opposition to Arguillat *et al.* [1], acoustic fluctuations cannot be separated from turbulent energy in our case. A new method based on Empirical Mode Decomposition in the spatial domain was shown to be able to increase

the separation capabilities of the spatial correlogram on uniform and stationary flow. This was clearly illustrated using an artificial noise source in the wind tunnel. Nevertheless, this is not efficient enough for extracting the TBL noise itself, nor the detached-reattached flow noise. Furthermore, the spatial correlogram method, even “enhanced” by sEMD, is still unsuitable for non-uniform and non-stationary flow. The next step will be to develop a new instantaneous method, the Ensemble-EMD (E-EMD), that will allow us to quantify a maximum threshold for acoustic energy produced by the flow at each instant.

Acknowledgments

The authors would like to thank Vincent Grulier from “GIPSA-Lab” (GRENOBLE) for his great help with EMD codes, and Laurent Philippon, Patrick Brau and Pascal Bias from the “Laboratoire d’Études Aérodynamiques” (POITIERS) and Yves Corvez from PSA-PEUGEOT-CITROËN for their advice and technical help.

References

- [1] B. Arguillat, D. Ricot, G. Robert, C. Bailly, “Measurements of the wavenumber-frequency spectrum of wall-pressure fluctuations under turbulent flows”, *11th AIAA/CEAS Aeroacoustics Conf. Monterey CA. AIAA Paper*, (2005).
- [2] S. Debert, M. Pachebat, V. Valeau, Y. Gervais, “Experimental wave number separation of wall-pressure fluctuations beneath a Turbulent Boundary Layer”, *Inter. Congress on Acoustics Madrid*, (2007).
- [3] P. Flandrin, G. Rilling, P. Goncalves, “Empirical Mode Decomposition as a Filter Bank”, *IEEE Signal Processing Letters* 11, 112–114, (2004).
- [4] R. Garello, *Bi-dimensional Signal Analysis (Digital Signal and Image Processing series)*, ISTE, (2007).
- [5] V. Grulier, J. I. Mars, S. Debert, M. Pachebat, “Acoustic and turbulent wavenumbers separation in wall pressure array signals using emd in spatial domain”, *ICASSP 2008 Las Vegas*, (2008).
- [6] N. E. Huang, Z. Shen, S. R. Long, M. C. Wu, H. H. Shih, Q. Zheng, N.-C. Yen, C. C. Tung, H. H. Liu, “The empirical mode decomposition and the Hilbert spectrum for nonlinear and non-stationary time series analysis”, *The Royal Society of London* 454, 903–995, (1998).
- [7] H. Schlichting, *Boundary-Layer Theory*, McGraw-Hill, New-York, 7th Ed., (1979).
- [8] Z. Wu, N. E. Huang, “Ensemble empirical mode decomposition: A noise assisted data analysis method”, *Technical Report 173, Centre for Ocean-Land-Atmosphere Studies*, (2004).